Depletion attraction impairs the plasticity of emulsions flowing in a constriction†

Iaroslava Golovkova, [a] Lorraine Montel, [a] Elie Wandersman, [a] Thibault Bertrand, ⋆[b] Alexis Michel Prevost [a] and Lea-Laetitia Pontani ⋆[a]

We study the elasto-plastic behavior of dense attractive emulsions under a mechanical perturbation. The attraction is introduced through non-specific depletion interactions between the droplets and is controlled by changing the concentration of surfactant micelles in the continuous phase. We find that such attractive forces are not sufficient to induce any measurable modification on the scalings between the local packing fraction and the deformation of the droplets. However, when the emulsions are flowed through 2D microfluidic constrictions, we uncover a measurable effect of attraction on their elasto-plastic response. Indeed, we measure higher levels of deformation inside the constriction for attractive droplets. In addition, we show that these measurements correlate with droplet rearrangements that are spatially delayed in the constriction for higher attraction forces.

1 Introduction

The flow of particulate systems is a problem of great importance both theoretically and practically, with direct applications to the industry. It is relevant for a wide range of soft materials, from granular packings to foams and emulsions. While these materials present obvious differences, they share universal features, *e.g.* they generically undergo what is known as a jamming transition.[1,2] As the particle or droplet volume fraction ϕ increases, this rigidity transition between liquid and amorphous-solid states controls the phase behavior of these disordered solids. At a critical volume fraction ϕ_c (random close packing), the system jams and develops a yield stress.[3–6] The mechanical and rheological properties, such as the elastic modulus or the local pressure, of these systems are known to display a power law dependence with the distance to the jamming onset $(\phi - \phi_c)$.[4,5,7–12]

Jammed solids are characterised by a spatially heterogeneous network of interparticle contacts, with a broad distribution of contact forces exhibiting an exponential tail[4,11,13,14] in which only a small subset of the particles sustain most of the mechanical load.[15–18] Below the yield stress, these systems respond elastically, while above it, they deform and flow plastically.[19] In these soft glassy flows, it was shown that stress and strain rates are coupled nonlocally.[6,20,21] In two-dimensional materials, the

flow properties can easily be probed both at the microscopic and macroscopic scales.[22–31] As a consequence, previous experimental studies examined the microscopic rearrangements in a variety of two-dimensional model systems under stress.[32,33] This plastic flow is generically governed by local structural rearrangements which relieve stresses and dissipate energy.[6,22,23,34] Local plastic rearrangements have been connected to the fluctuating macroscopic flow in both simulations[35–39] and theoretical studies[6,20,21,40,41] of model systems. Nevertheless, the intimate link between the microscopic dynamics of an amorphous material and its macroscopic elasto-plastic response is still an open question for a broad class of more realistic materials.

In emulsions, the use of surfactants prevents the coalescence of the droplets and leads to short-range purely repulsive droplet–droplet interactions.[22,23,42] As such, dense stable emulsions are examples of jammed solids. In the last decades, a number of experimental works studied the structural, mechanical and rheological properties of purely repulsive emulsions.[12,42–47] In particular, as in other soft materials,[29,31,48–52] recent studies in quasi-2D flowing emulsions have also highlighted the importance of T1 events for local rearrangements and stress redistribution.[22,23] Monodisperse emulsions allow one to study material properties such as grain boundaries, dislocations and plasticity;[53–57] in particular, a recent study showed the existence of a spatiotemporal periodicity in the dislocation dynamics of these emulsions.[33] However, none of these studies have so far addressed the question of how interdroplet attractive forces modify the flow response of these emulsions.

Indeed, in a variety of natural settings and industrial applications, emulsion droplets do display additional attractive interactions that have been shown to change the nature of

[a] *Sorbonne Université, CNRS, Institut de Biologie Paris-Seine (IBPS), Laboratoire Jean Perrin (LJP), F-75005, Paris, France. E-mail: lea-laetitia.pontani@sorbonne-universite.fr*

[b] *Department of Mathematics, Imperial College London, South Kensington Campus, London SW7 2AZ, UK. E-mail: t.bertrand@imperial.ac.uk*

† Electronic supplementary information (ESI) available. See DOI: 10.1039/c9sm02343g

the jamming transition.[58–60] In contrast with the purely repulsive case, droplets in attractive emulsions can form bonds and thus a soft gel-like elastic structure which can sustain shear stresses below isostaticity.[45,61–63] However, the microscopic dynamics of the material, *i.e.* at the scale of the particles, was not explored. As a consequence, it is of particular importance to ask how the response to stress and in particular, the structural and mechanical properties of emulsions are modified by the presence of attractive interactions. Despite their broad applicability, our understanding of the influence of particle–particle interactions on the macroscopic properties of soft matter systems with attractive interactions is currently hindered by a crucial lack of controlled experimental settings.

In this article, we propose a first step towards completing our understanding of the microscopic origin for the macroscopic properties of adhesive emulsions. In particular, we study emulsions in which droplets interact through depletion attraction. First, we find that the static structure of 2D polydisperse emulsions remains unchanged by the introduction of depletion forces. However, the response of 2D monodisperse emulsions under mechanical constraint is impacted by the presence of depletion forces. Indeed, we flow the droplets through a microfluidic constriction in which they have to undergo elasto-plastic remodelling in order to go from a wide channel to a narrow one. In particular, we find that attractive droplets deform more inside the constriction, which we correlate to a shift in the positions of rearrangements. These findings show that depletion attraction forces are sufficient to modify the elasto-plastic response of dense emulsions under a mechanical perturbation. This attraction, even though it is not evidenced in static conditions, impairs rearrangements and in turn promotes an enhanced elastic response under flow.

2 Materials and methods

2.1 Emulsion preparation

Polydisperse emulsions are prepared using a pressure emulsifier (Internal Pressure Type, SPG Technology Co.). Silicone oil (viscosity 50 mPa s, Sigma Aldrich) is pushed through a cylindrical Shirasu Porous Glass membrane decorated with 10 μm pores, directly into a 10 mM SDS solution that is maintained under vigorous agitation. The resulting droplets display an average diameter of 42 μm (polydispersity 21%). In order to prepare the emulsion with both SDS concentrations, we use the same droplets and only replace their continuous phase. To do so, the emulsion is washed in a separating funnel in order to replace the continuous phase by solutions of 10 or 45 mM SDS in a water/glycerol mixture (60:40 in volume). This enhances the optical quality of the oil/water interface visualization through bright field and confocal microscopy.

For experiments in the constriction and in static packings, we use monodisperse emulsions with an average droplet diameter of 45 μm (polydispersity 3.9%). These emulsions are obtained with a custom made flow-focusing microfluidic set-up (channel size 60 μm × 60 μm, width at the flow-focusing junction 30 μm). We use the same oil and continuous phases for polydisperse and monodisperse emulsions.

2.2 Observation and image analysis of 2D static packings

When studying 2D static packings, we consider emulsions that are fluorescently labelled with Nile Red (Sigma Aldrich). To label the emulsion, we incubate it overnight in a SDS buffer (with [SDS] = 10 or 45 mM) saturated in Nile Red allowing the dye to partition between the oil and water phases over time. A 10 μL drop of emulsion is placed between a microscope glass slide (76 × 26 mm, Objekttrager) and a cover slip (24 × 60 mm, Knittel Glaser) separated by spacers (50 μm or 30 μm polymethylmethacrilate – PMMA-film, Goodfellow). Droplets are imaged through confocal microscopy (Spinning Disc Xlight V2, Gataca systems) using a 20× objective.

To study the local structure of these static packings, we use a custom Matlab (MathWorks) routine that works as follows. We first threshold the images and perform a watershed tessellation, we then measure the perimeter p and area a of each droplet as well as the area a_c of the associated watershed tesselation cell (see Fig. 1D). Following Boromand *et al.*,[64] we study the relation between the deformation of the droplets and their local packing fraction. To do so, we compute their shape factor $\mathscr{A} = p^2/4\pi a$ and determine the local packing fraction $\phi_l = a/a_c$. Note that we only consider droplets in the center of the packing, *i.e.* we exclude those that are partially cut by the edge of the image frame. The shape parameter $\mathscr{A}$ equals 1 for circular disks and is greater than 1 for all nonspherical particles.[65]

2.3 Experimental set-up for emulsion flow

We designed the constriction in a microfluidic channel composed of three main sections (Fig. 1): at the entrance, the channel is 50 μm deep and 200 μm wide over a 5 mm length, then at the constriction the width is reduced from 200 to 50 μm over a length of 200 μm, finally the channel remains 50 μm wide over a final 5 mm length. Note that the droplets are not confined in the vertical direction in this geometry since their diameter is slightly smaller than the height of the channel. The channel is made in polydimethylsiloxane using a negative cast micromachined in a block of PMMA (50 × 50 × 5 mm³) using a desktop CNC Mini-Mill machine (Minitech Machinary Corp., USA). After passivating the channel with casein 0.05 mg mL⁻¹ (β-casein from bovine milk, Sigma Aldrich) for 20 minutes, the emulsion is flowed in the device using a pressure pump (MFCS-8C Fluigent, P = 30 mbar). After droplets fill the constriction area, the pressure is decreased to stop the emulsion flow, and droplets are left to cream in the supply tube overnight, thus compressing the droplets in the microfluidic device in order to reach high values of packing fraction. After this passive compression phase, the emulsion is flowed again in the channel at a constant pressure. The flow of the droplets at the constriction is imaged in bright field microscopy with a 10× objective at a frequency of 20 frames per second (fps).

2.4 Image analysis of the emulsions flowing in the constriction

To analyse the videos of flowing emulsions, we first threshold the images to subsequently determine the center and perimeter
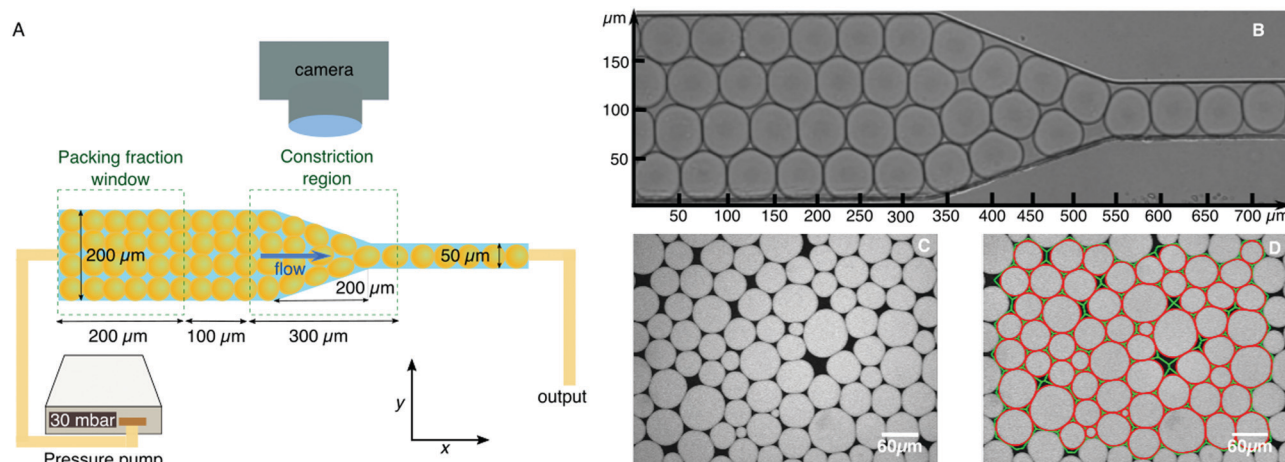
Fig. 1 Experimental set-up and image analysis – (A) the oil in water emulsion is pushed using a pressure pump ($P = 30$ mbar) through the microfluidic channel that consists of three parts: a 200 μm wide channel, a constriction, and a 50 μm wide channel. The depth of the channel is 50 μm over the whole length, and the diameter of the droplets is ≈ 45 μm. (B) Typical image of a monodisperse emulsion flowing in the constriction. In the area of the constriction, the flow of the droplets is imaged in bright field microscopy at 20 fps. The packing fraction of the emulsion is determined within the window of 200 × 200 μm located before the constriction area. (C) A typical confocal microscopy image of compressed 2D droplets at [SDS] = 10 mM. (D) Result of the image analysis performed on (C). Droplet contours are shown in red and watershed tessellation cells with the green curves. Based on these measurements, we calculate the local packing fraction ϕ_l as the ratio between the area of the droplet and that of its corresponding watershed tesselation cell, as well as the shape parameter $\mathscr{A}$.

of each droplet in the channel using a custom made Matlab routine. When studying droplet deformation, we only consider the droplets located in the constriction region. We define this area along the channel as a window that includes the 200 μm of the constriction itself, plus 50 μm before and after the constriction (Fig. 1). To quantify the deformation of each droplet, we use the approach proposed by Chen *et al.*[23] The perimeter of the droplet is interpolated and discretized at 1024 evenly spaced angles θ and the deformation d is calculated as a standard deviation of the radii $r(\theta)$ for each of these angles divided by the mean value of r:

$$d = \frac{\sqrt{\langle r^2 \rangle - \langle r \rangle^2}}{\langle r \rangle} \quad (1)$$

We also determine the global packing fraction of the emulsion in each video frame. To this end, we calculate the ratio between the sum of all droplets area and the area of the channel within the window of 200 × 200 μm located before the constriction region. Finally, frames are sorted according to the emulsion packing fraction, and the distributions of droplet deformations for each packing fraction are computed.

For rearrangements and flow analysis, the droplets were tracked using a custom Python routine and the FastTrack software (http://www.fasttrack.sh/). All droplets are sorted according to the lane they belong to in the channel ahead of the constriction. In our experiments, they are thus sorted into four lanes. The instantaneous velocity of the droplets was computed as the distance travelled between two consecutive frames acquired at a fixed frame rate $v(t) = \frac{\sqrt{(x(t+\mathrm{d}t) - x(t))^2 + (y(t+\mathrm{d}t) - y(t))^2}}{\mathrm{d}t}$. In our images the spatial resolution yields 300 nm per pixel.

3 Results

3.1 Analysis of static packings

We first study 2D static packings of monodisperse and polydisperse emulsions with two distinct depletion interactions. Using silicon oil droplets stabilized with two different concentrations of SDS (10 mM and 45 mM) allows us to change the depletion forces between the droplets. In our experiment, the continuous aqueous phase is supplemented in glycerol (40% in volume of glycerol). Note that in addition to allowing for a better imaging of the droplets, it also shifts the critical micellar concentration (CMC) of SDS. However, the CMC is only raised from 8 mM (in pure water) to about 9 mM in our experimental conditions,[66,67] which ensures that the system is still above the CMC under both SDS concentrations and that the surface tension remains the same when the concentration of SDS is increased from 10 to 45 mM. Above the CMC, depletion attraction forces increase linearly with the concentration of micelles,[68] which itself grows with increasing concentrations of SDS. Given the aggregation numbers of SDS (*i.e.* the number of SDS molecule per micelle at a given concentration) found in the literature,[69–71] we estimate that there is approximately 30 times more micelles at 45 mM SDS than at 10 mM SDS (see ESI†). Depletion forces at 45 mM SDS are thus expected to be 30 times larger than at 10 mM SDS.

To study the impact of depletion forces on static 2D packings, we first quantify the deformation of the droplets as a function of their local packing fraction in these monodisperse and polydisperse emulsions. Thus, we measure the asphericity and local packing fraction of each droplet in several images of 2D monodisperse and polydisperse packings for both 10 and 45 mM SDS concentrations (see Materials and methods).

In Fig. 2A, we first plot ϕ_l *vs.* $\mathscr{A} - 1$ for monodisperse emulsions for both SDS concentrations. Surprisingly, we find that data for both SDS concentrations are collapsing on the same master curve showing that the depletion-induced attractive interactions between the droplets have little effect on the structure of static packings.

To confirm the results we obtained for monodisperse emulsions, we also performed experiments on disordered packings (see Fig. 1C and D for an example of polydisperse emulsion). In Fig. 2B, we plot ϕ_l *vs.* $\mathscr{A} - 1$ for polydisperse emulsions for both SDS concentrations. Recent studies[64,65] developed a new numerical model to study the structural and mechanical properties of disordered 2D packings of bubbles and emulsions, including at high compressions. In the so-called deformable particle (DP) model, particles deform in response to mechanical constraints to minimize their perimeter while keeping their area fixed. This leads to a model of deformable disks with potential energies that include an energy term associated to the line tension and a penalization energy term quadratic in the change of area of the droplets, thus associated to their compressibility. Further, the deformable particles interact *via* a purely repulsive potential energy. Within the framework of this DP model and in our range of deformations, it was predicted that for disordered packings the distance to jamming onset $\phi_l - \phi_c$ scales with asphericity $\mathscr{A} - 1$ as

$$\phi_l - \phi_c = \alpha(\mathscr{A} - 1)^{\omega} \qquad (2)$$

with $\omega \approx 0.3$.

In the case of the disordered packings, we can compare our experimental data to this theoretical prediction. We find that the data for both SDS concentrations are well-fitted by eqn (2) with scaling exponent $\omega = 0.33$ and critical volume fraction $\phi_c = 0.842$, *i.e.* the scaling form obtained in the DP model. A summary of the fitting procedure and a table of all performed fits for both SDS concentrations are given in ESI.† While the results of the DP model were obtained for disordered systems, we also find that the change in local packing fraction as a function of droplet deformation in monodisperse emulsions is well described by the power law scaling in eqn (2) with, in this case, a scaling exponent $\omega \approx 0.25$ and a critical packing fraction $\phi_c = 0.91$ which can be explained by a high degree of crystallization.

These scalings are shown on a log–log scale in Fig. 2C, where we show that, in monodisperse emulsions (respectively polydisperse emulsions), data points corresponding to both depletion forces overlap and are captured by the same scaling function with $\phi_c = 0.91$ and $\omega = 0.25$ (respectively $\phi_c = 0.842$ and $\omega = 0.33$). This indicates that depletion induced attractive interactions do not affect significantly the scaling $\phi_l - \phi_c$ *versus* $\mathscr{A} - 1$, *i.e.* changing SDS concentration does not induce any measurable modification in the static packings of droplets. This might seem counterintuitive. Indeed, while it was shown that purely repulsive polydisperse emulsions become fluid-like below random close packing (*i.e.* only respond elastically above random close packing), experimental studies on the rheology of attractive emulsions showed that attractive emulsions are
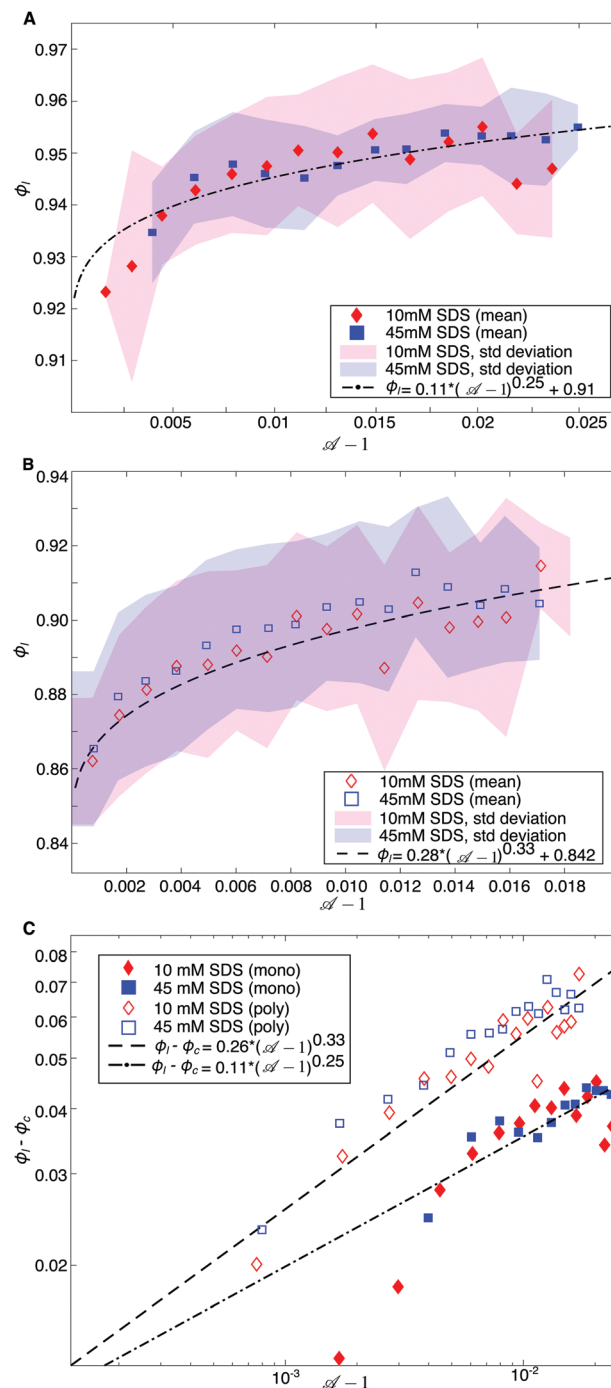

Fig. 2 Analysis of static 2D packings – local packing fraction ϕ_l *versus* $\mathscr{A} - 1$ for monodisperse (A) and polydisperse (B) emulsions. In (A), the experimental points (red diamonds for 10 mM SDS, blue squares for 45 mM SDS) are plotted together with the scaling function in eqn (2) with exponent $\omega = 0.25$ and $\phi_c = 0.91$ (black dot-dashed line). In (B), the experimental points (red open diamonds for 10 mM SDS, blue open squares for 45 mM SDS) are plotted together with the DP model, *i.e.* scaling function in eqn (2) with exponent $\omega = 1/3$ and $\phi_c = 0.842$ (black dashed line). (C) Log–log plot of $\phi_l - \phi_c$ *versus* $\mathscr{A} - 1$ for monodisperse and polydisperse emulsions for both SDS concentrations. We used $\phi_c = 0.91$ and $\phi_c = 0.842$ for mono and polydisperse packings respectively. The total number of droplets for: (1) polydisperse emulsions are $N = 1193$ and $N = 1735$ for 10 and 45 mM SDS respectively and (2) monodisperse emulsions are $N = 630$ and $N = 530$ for 10 and 45 mM SDS respectively.

elastic both below and above random close packing hinting at the fact that loose emulsions can be stabilized by attraction.[63] Here, we do not observe any significant change in ϕ_c for static packings with depletion interactions. In our SDS stabilized emulsions, the droplets are essentially frictionless and thus are free to roll. In such a system, the slightest amount of compression will lead to a rearrangement of the structure without noticeable deformation of the droplets until their purely repulsive jamming packing fraction is reached. This intuition is confirmed by the measured values of ϕ_c which correspond to random close packing $\phi_{RCP} \approx 0.842$ for the polydisperse (disordered) emulsions and to hexagonal close packing $\phi_{HCP} = 0.91$ for the monodisperse emulsions.

Despite the fact that static packings cannot be distinguished as a function of depletion forces, we reveal in what follows that significantly distinct behaviors can be evidenced in the context of a dynamic flow.

3.2 Emulsion flow in a constriction

In order to study their response under mechanical perturbations, monodisperse emulsions are flowed in microfluidic channels exhibiting a single physical constriction (Fig. 1). In particular, we use monodisperse droplets whose diameter is comparable to the channel height, constraining the system to a 2D monolayer of droplets. We focus our analysis on the area of the constriction in which droplets have to rearrange and deform in order to go from a large channel into a narrower one. The width of the narrow channel is chosen such that it only allows for the passage of one droplet diameter (Fig. 1) in order to maximize the number of rearrangements.

A typical experiment is carried out in two phases. The channel is first filled with the emulsion using a pressure pump. After a waiting time (see Materials and methods), the pressure is increased again so that this packed emulsion can flow in the channel. We usually require a typical pressure of the order of 30 mbar to establish a continuous flow. For each experiment, we image the droplets upstream, in order to evaluate their packing fraction, as well as inside the constriction to measure their deformation. We choose to quantify the deformation d of each droplet in the channel through the standard deviation of droplet radii as previously done[23] (see Materials and methods).

3.3 Deformation along the channel

We first study the deformation of the droplets inside the channel. To do so, we measure the packing fraction of the emulsion in a window located upstream of the constriction (on the left of the image) and that encompasses 200 µm of the channel length (Fig. 3A). We show in Fig. 3 the average deformation $\langle d \rangle$ along the channel for both SDS concentrations.

The obtained curves differ for the two SDS concentrations both in the constriction region and in the thinner channel. For both conditions (Fig. 3B and C) the deformation builds up in the constriction to a first maximum average deformation until it is released to a lower value of $\langle d \rangle$ at $x \approx 450$ µm. Then the deformation builds up again to a second maximum and is decreased to a lower deformation. Qualitatively, this behavior
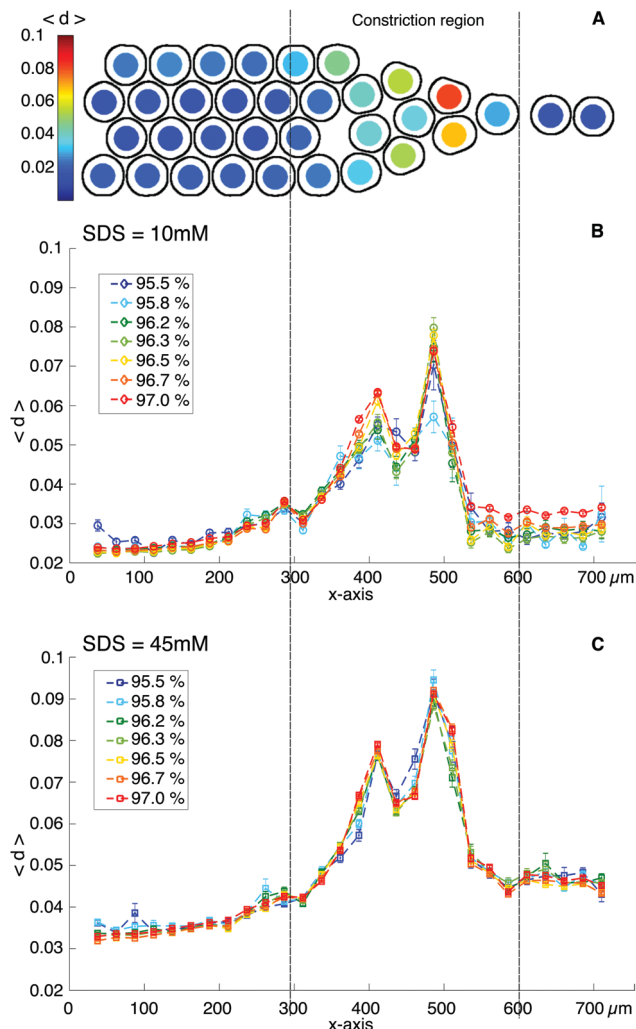

Fig. 3 Analyzing the droplet deformation in the constriction – (A) still snapshot of the image analysis in the channel at a given instant for an attractive emulsion ([SDS] = 45 mM). The color of the droplets codes for their deformation d calculated for their detected contours displayed on the image. (B and C) Average deformation of the droplets along the x-axis of the channel for different packing fractions in (B) the low attraction case ([SDS] = 10 mM) and (C) high attraction case ([SDS] = 45 mM). The deformation is averaged in bins that are 25 µm wide along the x-axis. The average deformation peaks inside the area of the constriction for both conditions. The error bars correspond to the standard error of the mean for the distributions of d obtained in each bin. The total number of droplets, combining all packing fractions, is $N = 27\,219$ for 10 mM SDS and $N = 91\,391$ for 45 mM SDS.

can be explained as the signature of a local stress release after a rearrangement. Indeed, Chen *et al.*[23] showed that in compressed emulsions, T1 events were immediately followed by a local decrease of deformation inside compressed emulsions. Here the localized peaks indicate that droplet rearrangements indeed occur at positions that are set by the topology of the packing in the channel.[33]

The other difference between the two conditions can be observed in the thinner channel region, after the constriction, where droplets enter one by one and release their deformation. In the case of low depletion forces ([SDS] = 10 mM), droplets

relax to a deformation value that is close to the initial one at the entry of the channel ($\langle d \rangle_{\text{out}} - \langle d \rangle_{\text{in}} \approx 0.0025$). However, with high depletion forces ([SDS] = 45 mM), droplets relax to a plateau at higher values of deformation than at the entry ($\langle d \rangle_{\text{out}} - \langle d \rangle_{\text{in}} \approx 0.01$). This impaired relaxation could be a signature of long range effects that could also explain why droplets enter the constriction with a slightly higher value of deformation in the high attraction case.

3.4 Deformation as a function of packing fraction

To further confirm these observations, we study the distribution of deformation of all droplets at all positions inside the constriction (taken in a window whose length spans 50 μm before and after the constriction – see Materials and methods). Since the global packing fraction can evolve over the course of one experiment, we separate each experiment into stacks according to their upstream packing fraction. We then pool together the image sequences corresponding to the same packing fraction throughout all performed experiments, for each concentration. Note that we also checked that the deformation in the constriction does not depend on the instantaneous droplet velocity within the investigated range (from 120 to 360 μm s^{-1}, see ESI†).

We compare the distributions of the deformations observed for different packing fractions and for each SDS concentration (Fig. 4). The distributions peak at smaller values of deformation in the low attraction case than in the case of strongly attractive droplets (Fig. 4A). This shift can also be clearly evidenced when plotting the cumulative distributions for each condition at various packing fractions (see Fig. 4B). As expected, for low depletion forces (10 mM SDS) we find that the distributions exhibit lower values of deformation in all conditions. When attraction is introduced between droplets, all curves are shifted to higher values of deformation.

In the previous section we showed that depletion alone was not sufficient to induce significant additional deformations in static packings of droplets. The shift observed in these deformation distributions must thus originate from differences in the local topological changes of the emulsions. Hence, we next examine the spatial location of rearrangements in the constriction as a function of SDS concentration.

3.5 Rearrangements and velocity distributions in the constriction

We here test the hypothesis that rearrangements are impaired by the attraction between the droplets, which would in turn force the droplets to deform more to overcome the constriction.

Since the size of the channel as well as the diameter of the droplets are fixed, there are always four lines of droplets flowing in the channel, ahead of the constriction, and one line after the constriction (Fig. 5A). In this framework, droplets will exchange neighbors to do the necessary rearrangements in given areas of the channel that are defined by geometry. We can thus estimate the distance Δx between two rearrangements by calculating the distance between the points where one can accommodate for 4 droplets and 3 droplets of diameter D in the
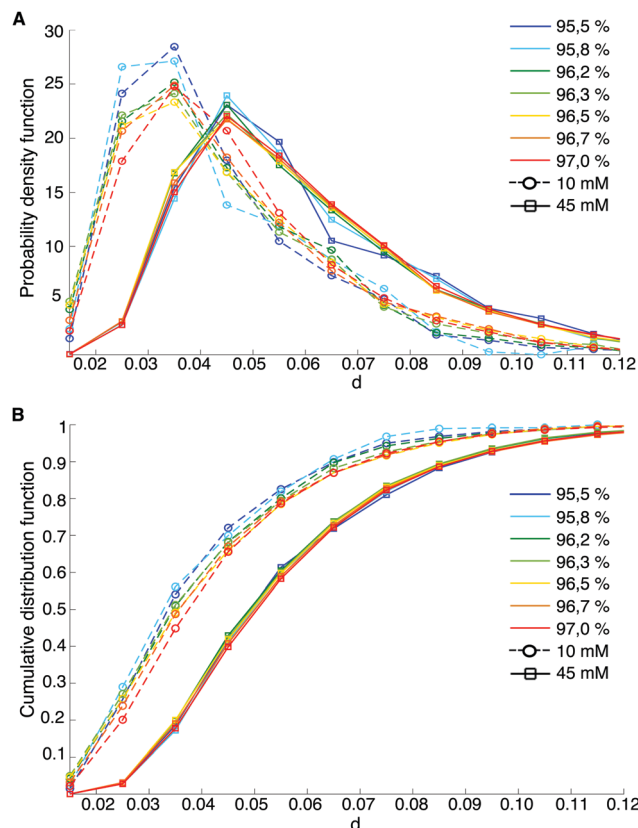

Fig. 4 Statistics of deformation under flow – (A) probability density function of the deformation d calculated in the constriction for different packing fractions in the case of low attraction forces ([SDS] = 10 mM, open circles) and high attraction forces ([SDS] = 45 mM, stars). (B) Cumulative distributions of the deformation d in the constriction for low attraction forces (open circles) and high depletion forces (open squares) for different packing fractions.

constriction. Knowing the slope of the constriction α this leads to $\Delta x = D/(2\alpha) = 60$ μm.

To study these rearrangements, we measure both the velocity and number of neighbors of the droplets along the channel. In the constriction, droplets are stalled transiently until they perform a rearrangement. This effect is evidenced by local minima in their individual velocity profiles as shown in Fig. 5B, that are separated by the expected distance between rearrangements Δx. We extract the positions of these minima in two specific areas of the channel, corresponding to zones of rearrangements, for each droplet in lines 1 and 4 for both SDS concentrations. We compare both conditions by plotting the cumulative distributions of the minimum velocity location in each zone (Fig. 5C). We observe that the distributions for attractive droplets are shifted by 7 μm and 4 μm in zones 1 and 2 respectively (measured shift at 50%), indicating that rearrangements are indeed delayed in the channel compared to the low depletion case. Similarly to the deformation, this shift does not seem to depend on the flow speed in the channel (see ESI†).

Furthermore, we analyzed the average number of neighbors per droplet along the constriction (Fig. 5D). Droplets in lines 1
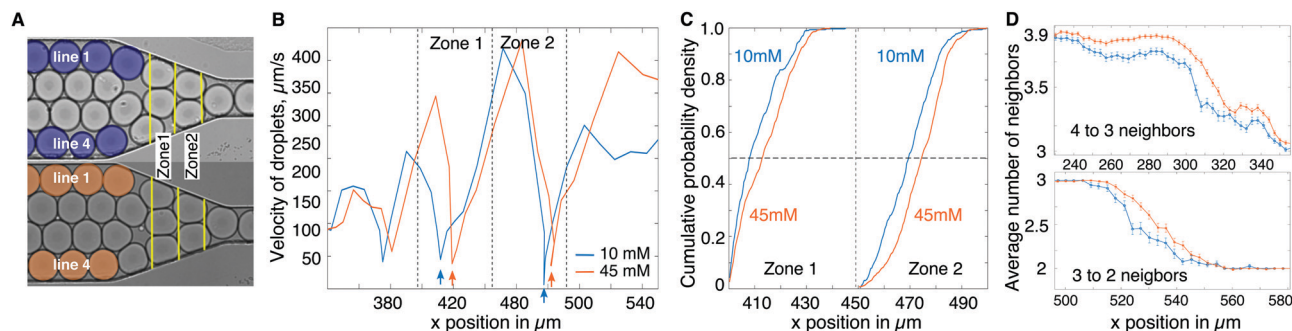
Fig. 5 Rearrangements and velocity distributions in the constriction – (A) image of droplets in the constriction for 10 mM (top, blue) and 45 mM (bottom, orange) SDS. The zones where the number of droplets decreases from 3 to 2 and from 2 to 1 are indicated with yellow lines and referred to as zone 1 and 2 respectively. (B) Typical velocity curves of individual droplets in lines 1 and 4 along the channel axis for 10 mM (blue) and 45 mM SDS (orange) emulsions. The velocity drops to a minimum value (indicated by an arrow) in zones 1 and 2 each time the droplets stall before a rearrangement. For each droplet trajectory we find the location of this minimal velocity to build panel (C). (C) Cumulative distributions of the minimum velocity location for lines 1 and 4. The 45 mM SDS droplets slow down farther into the constriction, as evidenced by the shift in distributions at 50% probability, by about 7 μm in zone 1 and 4 μm in zone 2. (D) Average number of neighbors per droplet along the channel for lines 1 and 4. For more attractive emulsions, the number of neighbors drops from 4 to 3 and then from 3 to 2 respectively 11 μm and 8.5 μm later in the constriction.

and 4 enter the constriction with 4 neighbors in a hexagonal lattice, and exit with 2 neighbors in the smaller channel. We measured the positions along the channel where droplets transition on average from 4 to 3 and from 3 to 2 neighbors respectively. We find that, for the more attractive emulsions, the transitions from 4 to 3 and from 3 to 2 neighbors are delayed by 11 μm and 8.5 μm respectively.

4 Discussion

Attractive interactions between particles are expected to affect their packing topology as well as their rheological and mechanical response to local mechanical perturbations. Below the jamming transition, previous work showed that attraction induced by depletion forces tuned significantly the structure of 3D packings and could mechanically stabilize them below the isostatic limit.[60] Above the jamming transition, one expects adhesive forces in packings of deformable spheres to change how droplet deformation and coordination numbers scale with the packing fraction.[64,65] To the best of our knowledge, this issue has been addressed neither in theoretical models nor in experimental systems.

In our experimental study, we provide a first step towards the understanding of the mechanical response of adhesive emulsions by introducing attractive interactions induced by depletion between oil droplets. We first evidence that such attraction forces are too low to induce any measurable effect in 2D static packings of droplets. Indeed, for both attraction forces, we recover the scaling laws predicted by Boromand *et al.*[64] for purely repulsive packings, with a critical packing fraction $\phi_c \approx 0.842$. However, using monodisperse emulsions, we uncovered distinct changes in their elasto-plastic response when the droplets are flowed through a 2D physical constriction. Note that recent numerical studies dealing with attractive soft sphere packings showed similarly that attractive packings with structures very similar to their repulsive counterpart

(*e.g.* in the fact that the critical packing fraction is not significantly different) could have qualitatively different mechanical properties.[72] In our experiments, the first manifestation of attraction is an increase of the average deformation of the droplets in the constriction. The second one is the delay of topological rearrangements inside the constriction as attraction forces are increased. Depletion forces thus appear adequate to modulate the elasto-plastic response of emulsions in our system.

Such findings could be relevant for biological tissues in which adhesion controls to a large extent remodelling events that occur on timescales that are beyond those of cytoskeletal activity. In order to isolate the role of adhesion in biological processes, cellular tissues can indeed be mimicked with droplet assemblies connected by specific binders.[73–75] Within that framework, emulsions have been shown to exhibit similar mechanical properties and have for this reason been used to measure cellular forces both *in vitro*[76] and *in vivo*.[77,78] This reductionist approach could thus shed light on behavioral transitions in developing tissues upon adhesion modulation and will be the focus of future investigations.

Conflicts of interest

There are no conflicts to declare.

Acknowledgements

References

1 A. J. Liu and S. R. Nagel, *Annu. Rev. Condens. Matter Phys.*, 2010, **1**, 347–369.

2 M. van Hecke, *J. Phys.: Condens. Matter*, 2009, **22**, 033101.

3 M. E. Cates, J. P. Wittmer, J.-P. Bouchaud and P. Claudin, *Phys. Rev. Lett.*, 1998, **81**, 1841–1844.

4 C. S. O'Hern, L. E. Silbert, A. J. Liu and S. R. Nagel, *Phys. Rev. E: Stat., Nonlinear, Soft Matter Phys.*, 2003, **68**, 011306.

5 P. Olsson and S. Teitel, *Phys. Rev. Lett.*, 2007, **99**, 178001.

6 J. Goyon, A. Colin, G. Ovarlez, A. Ajdari and L. Bocquet, *Nature*, 2008, **454**, 84.

7 C. S. O'Hern, S. A. Langer, A. J. Liu and S. R. Nagel, *Phys. Rev. Lett.*, 2002, **88**, 075507.

8 T. G. Mason, J. Bibette and D. A. Weitz, *Phys. Rev. Lett.*, 1995, **75**, 2051–2054.

9 M.-D. Lacasse, G. S. Grest, D. Levine, T. G. Mason and D. A. Weitz, *Phys. Rev. Lett.*, 1996, **76**, 3448–3451.

10 W. G. Ellenbroek, E. Somfai, M. van Hecke and W. van Saarloos, *Phys. Rev. Lett.*, 2006, **97**, 258001.

11 T. S. Majmudar, M. Sperl, S. Luding and R. P. Behringer, *Phys. Rev. Lett.*, 2007, **98**, 058001.

12 I. Jorjadze, L.-L. Pontani and J. Brujic, *Phys. Rev. Lett.*, 2013, **110**, 048302.

13 H. M. Jaeger, S. R. Nagel and R. P. Behringer, *Rev. Mod. Phys.*, 1996, **68**, 1259–1273.

14 J. Brujić, S. F. Edwards, I. Hopkinson and H. A. Makse, *Phys. A*, 2003, **327**, 201–212.

15 C. h. Liu, S. R. Nagel, D. A. Schecter, S. N. Coppersmith, S. Majumdar, O. Narayan and T. A. Witten, *Science*, 1995, **269**, 513–515.

16 M. E. Cates, J. P. Wittmer, J.-P. Bouchaud and P. Claudin, *Chaos*, 1999, **9**, 511–522.

17 T. S. Majmudar and R. P. Behringer, *Nature*, 2005, **435**, 1079–1082.

18 J. Zhou, S. Long, Q. Wang and A. D. Dinsmore, *Science*, 2006, **312**, 1631–1633.

19 D. T. Chen, Q. Wen, P. A. Janmey, J. C. Crocker and A. G. Yodh, *Annu. Rev. Condens. Matter Phys.*, 2010, **1**, 301–322.

20 K. Kamrin and G. Koval, *Phys. Rev. Lett.*, 2012, **108**, 178301.

21 L. Bocquet, A. Colin and A. Ajdari, *Phys. Rev. Lett.*, 2009, **103**, 036001.

22 K. W. Desmond and E. R. Weeks, *Phys. Rev. Lett.*, 2015, **115**, 098302.

23 D. Chen, K. W. Desmond and E. R. Weeks, *Phys. Rev. E: Stat., Nonlinear, Soft Matter Phys.*, 2015, **91**, 062306.

24 R. R. Hartley and R. P. Behringer, *Nature*, 2003, **421**, 928–931.

25 J. Lauridsen, G. Chanan and M. Dennin, *Phys. Rev. Lett.*, 2004, **93**, 018303.

26 A. Kabla, J. Scheibert and G. Debregeas, *J. Fluid Mech.*, 2007, **587**, 45–72.

27 B. Dollet and F. Graner, *J. Fluid Mech.*, 2007, **585**, 181–211.

28 B. Utter and R. P. Behringer, *Phys. Rev. Lett.*, 2008, **100**, 208302.

29 N. C. Keim and P. E. Arratia, *Phys. Rev. Lett.*, 2014, **112**, 028302.

30 N. C. Keim and P. E. Arratia, *Soft Matter*, 2015, **11**, 1539–1546.

31 J. Barés, D. Wang, D. Wang, T. Bertrand, C. S. O'Hern and R. P. Behringer, *Phys. Rev. E*, 2017, **96**, 052902.

32 J. Lauridsen, M. Twardos and M. Dennin, *Phys. Rev. Lett.*, 2002, **89**, 098303.

33 Y. Gai, C. M. Leong, W. Cai and S. K. Y. Tang, *Proc. Natl. Acad. Sci. U. S. A.*, 2016, **113**, 12082–12087.

34 A. Argon, *Acta Metall.*, 1979, **27**, 47–58.

35 D. J. Durian, *Phys. Rev. Lett.*, 1995, **75**, 4780–4783.

36 A. Kabla and G. Debrégeas, *Phys. Rev. Lett.*, 2003, **90**, 258303.

37 C. Maloney and A. Lematre, *Phys. Rev. Lett.*, 2004, **93**, 016001.

38 C. E. Maloney and A. Lematre, *Phys. Rev. E: Stat., Nonlinear, Soft Matter Phys.*, 2006, **74**, 016118.

39 V. Mansard, A. Colin, P. Chaudhuri and L. Bocquet, *Soft Matter*, 2013, **9**, 7489–7500.

40 M. L. Falk and J. S. Langer, *Phys. Rev. E: Stat. Phys., Plasmas, Fluids, Relat. Interdiscip. Top.*, 1998, **57**, 7192–7205.

41 G. Picard, A. Ajdari, F. Lequeux and L. Bocquet, *Eur. Phys. J. E: Soft Matter Biol. Phys.*, 2004, **15**, 371–381.

42 K. W. Desmond, P. J. Young, D. Chen and E. R. Weeks, *Soft Matter*, 2013, **9**, 3424–3436.

43 P. Hébraud, F. Lequeux, J. P. Munch and D. J. Pine, *Phys. Rev. Lett.*, 1997, **78**, 4657–4660.

44 P. Coussot, J. S. Raynaud, F. Bertrand, P. Moucheront, J. P. Guilbaud, H. T. Huynh, S. Jarny and D. Lesueur, *Phys. Rev. Lett.*, 2002, **88**, 218301.

45 L. Bécu, S. Manneville and A. Colin, *Phys. Rev. Lett.*, 2006, **96**, 138302.

46 P. Jop, V. Mansard, P. Chaudhuri, L. Bocquet and A. Colin, *Phys. Rev. Lett.*, 2012, **108**, 148301.

47 J. Lin, I. Jorjadze, L.-L. Pontani, M. Wyart and J. Brujic, *Phys. Rev. Lett.*, 2016, **117**, 208001.

48 M. Lundberg, K. Krishan, N. Xu, C. S. O'Hern and M. Dennin, *Phys. Rev. E: Stat., Nonlinear, Soft Matter Phys.*, 2008, **77**, 041505.

49 F. Graner, B. Dollet, C. Raufaste and P. Marmottant, *Eur. Phys. J. E: Soft Matter Biol. Phys.*, 2008, **25**, 349–369.

50 S. Cohen-Addad, R. Höhler and O. Pitois, *Annu. Rev. Fluid Mech.*, 2013, **45**, 241–267.

51 P. Marmottant, C. Raufaste and F. Graner, *Eur. Phys. J. E: Soft Matter Biol. Phys.*, 2008, **25**, 371–384.

52 D. Bi, J. H. Lopez, J. M. Schwarz and M. L. Manning, *Nat. Phys.*, 2015, **11**, 1074.

53 W. L. Bragg and J. F. Nye, *Proc. R. Soc. London, Ser. A*, 1947, **190**, 474–481.

54 P. Schall, I. Cohen, D. A. Weitz and F. Spaepen, *Science*, 2004, **305**, 1944–1948.

55 P. Schall, D. A. Weitz and F. Spaepen, *Science*, 2007, **318**, 1895–1899.

56 M. Arciniaga, C.-C. Kuo and M. Dennin, *Colloids Surf., A*, 2011, **382**, 36–41.

57 S. Arif, J.-C. Tsai and S. Hilgenfeldt, *J. Rheol.*, 2012, **56**, 485–499.

58 V. Trappe, V. Prasad, L. Cipelletti, P. N. Segre and D. A. Weitz, *Nature*, 2001, **411**, 772–775.

59 G. Lois, J. Blawzdziewicz and C. S. O'Hern, *Phys. Rev. Lett.*, 2008, **100**, 028001.

60 I. Jorjadze, L.-L. Pontani, K. A. Newhall and J. Brujić, *Proc. Natl. Acad. Sci. U. S. A.*, 2011, **108**, 4286–4291.

61 J. Bibette, T. G. Mason, H. Gang, D. A. Weitz and P. Poulin, *Langmuir*, 1993, **9**, 3352–3356.

62 P. Poulin, J. Bibette and D. Weitz, *Eur. Phys. J. B*, 1999, **7**, 277–281.

63 S. S. Datta, D. D. Gerrard, T. S. Rhodes, T. G. Mason and D. A. Weitz, *Phys. Rev. E: Stat., Nonlinear, Soft Matter Phys.*, 2011, **84**, 041404.

64 A. Boromand, A. Signoriello, J. Lowensohn, C. S. Orellana, E. R. Weeks, F. Ye, M. D. Shattuck and C. S. O'Hern, *Soft Matter*, 2019, **15**, 5854–5865.

65 A. Boromand, A. Signoriello, F. Ye, C. S. O'Hern and M. D. Shattuck, *Phys. Rev. Lett.*, 2018, **121**, 248003.

66 C. C. Ruiz, L. Diaz-Lopez and J. Aguiar, *J. Dispersion Sci. Technol.*, 2008, **29**, 266–273.

67 H. Khan, J. M. Seddon, R. V. Law, N. J. Brooks, E. Robles, J. T. Cabral and O. Ces, *J. Colloid Interface Sci.*, 2019, **538**, 75–82.

68 S. Asakura and F. Oosawa, *J. Polym. Sci.*, 1958, **33**, 183–192.

69 B. L. Bales, L. Messina, A. Vidal, M. Peric and O. R. Nascimento, *J. Phys. Chem. B*, 1998, **102**, 10347–10358.

70 B. Hammouda, *J. Res. Natl. Inst. Stand. Technol.*, 2013, **118**, 151–167.

71 G. Duplâtre, M. F. Ferreira Marques and M. da Graça Miguel, *J. Phys. Chem.*, 1996, **100**, 16608–16612.

72 D. J. Koeze and B. P. Tighe, *Phys. Rev. Lett.*, 2018, **121**, 188002.

73 L.-L. Pontani, I. Jorjadze, V. Viasnoff and J. Brujic, *Proc. Natl. Acad. Sci. U. S. A.*, 2012, **109**, 9839–9844.

74 L. Feng, L.-L. Pontani, R. Dreyfus, P. Chaikin and J. Brujic, *Soft Matter*, 2013, **9**, 9816.

75 L.-L. Pontani, I. Jorjadze and J. Brujic, *Biophys. J.*, 2016, **110**, 391–399.

76 D. Molino, S. Quignard, C. Gruget, F. Pincet, Y. Chen, M. Piel and J. Fattaccioli, *Sci. Rep.*, 2016, **6**, 29113.

77 O. Campàs, T. Mammoto, S. Hasso, R. A. Sperling, D. O'Connell, A. G. Bischof, R. Maas, D. A. Weitz, L. Mahadevan and D. E. Ingber, *Nat. Methods*, 2014, **11**, 183–189.

78 A. Mongera, P. Rowghanian, H. J. Gustafson, E. Shelton, D. A. Kealhofer, E. K. Carn, F. Serwane, A. A. Lucio, J. Giammona and O. Campàs, *Nature*, 2018, **561**, 401–405.